Optical fiber-based force transducer for microscale samples

Seshagiri Rao R. V.,[1,a)] Chirag Kalelkar,[2,b)] and Pramod A. Pullarkat[1,c)]
[1]*Biophysics Laboratory, Soft Condensed Matter Group, Raman Research Institute, Bangalore 560080, India*
[2]*Department of Mechanical Engineering, Indian Institute of Technology, Kharagpur 721302, India*

(Received 8 July 2013; accepted 20 September 2013; published online 11 October 2013)

We discuss the design, instrumentation, and calibration of a versatile force transducer with feedback control, called the Micro-Extensional Rheometer (MER). A force range of eight decades (1–10^8 pN) and a displacement range of four decades (10–10^5 nm) with a spatial resolution of the order of nanometers are accessible with the instrument. A feedback-loop algorithm is used to control the commanded force or the extensional strain on the sample and implement different rheometric protocols such as step-strain, step-force, exponential strain, among others. The device may also be used to measure the forces exerted by active suspensions, pulling neurons, etc. © *2013 AIP Publishing LLC*. [http://dx.doi.org/10.1063/1.4824198]

I. INTRODUCTION

During the last few decades, several advances have been made in force-measurement techniques at microscopic scales. Some of the more widely used force spectroscopy devices[1] include Atomic Force Microscopy (AFM),[2,3] optical tweezers,[4,5] and magnetic tweezers.[6,7] Apart from these techniques, several methods such as pulling neurons using micro-needles,[8,9] live-cell rheology using micro-plates,[10–12] stretching DNA using etched optical fibers[13] and magnetic beads,[14] micropipette-based force transducers,[15] MEMS-based force transducers,[16,17] etc., have been developed for specific applications. Many of these devices allow independent control of the force or the tensile strain depending on the mode of measurement. Each of these techniques have their advantages and disadvantages, which depend on the problem under consideration and the ease of fabrication or commercial availability. A large body of literature[1–17] is available which gives technical details and discusses utilitarian aspects of these methods.

Extensional properties of materials are important because extensional modes of deformation are obtained in a wide variety of industrial and laboratory settings, including tensile testing of materials, flow from an orifice, fiber-spinning of a thread, atomization involving breakup of liquid jets, flow through porous media, stagnation-point flows among others. In the field of extensional rheology,[18–20] some widely used methods for the study of materials such as polymer melts and solutions involve devices such as the Filament Stretching Extensional Rheometer (FiSER),[21,22] the Capillary Breakup Extensional Rheometer (CaBER),[23,24] Meissner-type elongational rheometer,[25] Sentmanat Extensional Rheometer,[26] etc. These devices operate at macroscopic scales and require a large volume of sample. Small-scale extensional rheometers include the microplate-based rheometer,[10–12] magnetic bead microrheometer,[27] etc. Material functions such as the uniaxial extensional modulus and the uniaxial extensional viscosity of the specimen are usually calculated.

In this paper, we describe a Micro-Extensional Rheometer (MER) which uses an etched optical fiber as a force-sensing cantilever. Optical-fiber cantilevers are easy to fabricate and do not require specialized equipment for manufacture, hence provide cost and time advantages. More importantly, the cylindrical geometry of the cantilever allows for quick and precise calibration. Force sensitivity can be easily tuned in the working range of 10^{-12} N to 10^{-4} N. Extensions of the order of 10^{-8} m to 10^{-4} m can be imposed with a displacement resolution of the order of tens of nanometers. Different modes of operation such as step-force, step-strain, or a specific force or strain protocol can be easily implemented. Simultaneous video microscopy with sub-micron resolution can be performed using phase-contrast, fluorescence or confocal modes of observation. Apart from applications involving the extensional rheology of polymer melts, we show that this setup can be used as a sensitive passive probe for exploring statistical properties of active media such as bacterial suspensions. We discuss the design of the apparatus, the calibration methods used for the components, some applications and compare our setup with other force-spectroscopy techniques and extensional rheometers.

II. EXPERIMENTAL SETUP

A. Instrumentation

We first provide a brief summary of the operating principles of the device and then supply details concerning technical aspects. A schematic diagram of the MER setup is shown in Fig. 1(a), along with a close-up view of the working area in Fig. 1(b). The working area comprises of a piezoelectric transducer and an optical fiber coupled to a laser, placed above the objective of a microscope. A cylindrical portion of the optical fiber acts as a cantilever for sensing the force. The length and diameter of the cantilever can be adjusted to achieve the desired force sensitivity. The tip of the cantilever is seen as a bright spot through the microscope, and a Position-Sensitive Detector (PSD) is used to track its motion or deflection. In the case of polymer melts, a picoliter-volume of the sample is placed within the gap between the tip of the cantilever and

[a)]Electronic mail: giripp@gmail.com
[b)]Electronic mail: kalelkar@mech.iitkgp.ernet.in
[c)]Electronic mail: pramod@rri.res.in

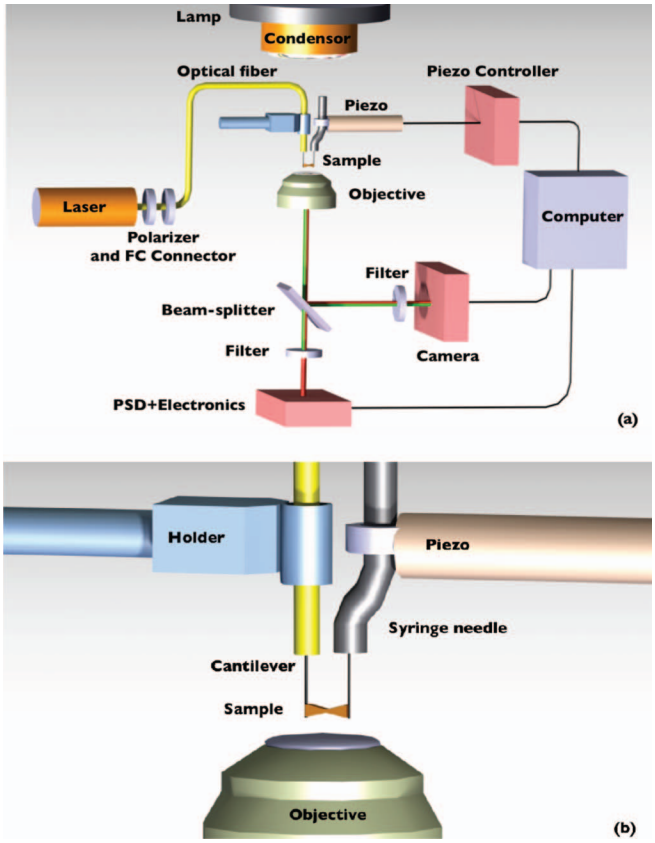

FIG. 1. (a) Schematic diagram of the Micro-Extensional Rheometer (MER), mounted on a vibration-isolation table. (b) A close-up view of the working area of the MER.

the end of a syringe needle (or any other suitable material of appropriate dimensions) attached to the piezo, as shown in Fig. 1(b). A lamp within the microscope is used to illuminate the sample through a condenser using green light, and images are recorded by a camera mounted on a side port of the microscope. Appropriate filters are used in front of the camera and the PSD to separate the green illumination light and the red laser light. The PSD reading and piezo control are obtained using a computer interface. Images are recorded and analyzed using custom-made software. We provide further technical details of the setup below.

The setup is mounted on a vibration-isolation table (VH3648W-OPT, Newport Corp., USA). A 17 mW, polarized, TEM_{00} He–Ne laser (25-LHR-925, CVI Melles-Griot, USA) with a beam diameter of 0.96 mm, operating at an output wavelength of 633 nm was used. The laser intensity is controlled by a linear polarizer (46 575, Edmund Optics, Singapore). The laser light is coupled to the optical fiber using an FC (Fiber-optic Connector) (F240FC-B, Thorlabs Inc., USA). The single-mode optical fiber (P1-630A-FC, Thorlabs Inc., USA) used has a mode field diameter (core) of 4.3 μm made of germanium-doped silica for a design wavelength of 633 nm, and a fiber outer diameter of 125 $\pm$ 1 μm made of silica. The tip of the cantilever as well as the sample are imaged using a microscope (Zeiss Observer.D1, Carl Zeiss GmbH, Germany) with a magnification 40 $\times$ /0.5. The sample is illuminated by green light using an interference filter placed above the microscope condenser. A beam-splitter sends 20% of the incident light to a side port mounted with a CCD camera (Andor Luca R604, Andor Technology, Ireland). A red-absorption filter is placed in front of the camera to attenuate the intensity of the laser light incident on it along with the scattered light (green) due to the sample for optimal simultaneous imaging. The CCD camera has a resolution of 1004(H)$\times$ 1002(V) pixels, a pixel size of (8 $\times$ 8) μm^2 and a frame rate of 12.4 Hz. For certain applications, a high-speed camera (MotionPro Y4, Integrated Design Tools Inc., USA) is available as an option. We used a pin-cushion type two-dimensional PSD (S2044, Hamamatsu Photonics, Japan) with an active area of (4.7 $\times$ 4.7) mm^2. The PSD was mounted with the detector surface coinciding with the image plane of the side port of the microscope which collects 80% of the light incident on the objective. A narrow bandpass interference filter (FL632.8-10, Thorlabs Inc., USA) placed in front of the detector allows only the laser light to be incident on the PSD. The PSD signal processing circuit (C9069, Hamamatsu Photonics, Japan) computes the position of the light spot, performs A/D conversion, and sends digital output at 200 Hz through a RS-232 interface to a computer. The PSD gives as output, the signal position and the incident light level in 12-bit hexadecimal format. A LabVIEW (Ver. 11, National Instruments, USA) code was used to record the PSD output and convert from hexadecimal to decimal. This code was tested against the application software of the PSD (Ver. 1.1, Hamamatsu Photonics, Japan). Position detection can also be performed using a Quadrant Photo-Diode (QPD) (QD-50-0, OSI Optoelectronics, USA) mounted on a side port of the microscope along with a 16-bit Data-Acquisition Card (PXIe-6363, National Instruments, USA). This device has a limited spatial range, but offers superior temporal resolution with a sampling rate up to 2 MHz. The piezo actuator (P-841.60, Physik Instruments GmbH, Germany) used for applying displacements has a 90 μm travel range, and comes with a single-axis piezo servo-controller (E-625.SR) having 24-bit A/D and 20-bit D/A resolutions. The actuator can sustain a pushing force up to 1000 N and a pulling force up to 50 N. The piezo is controlled using the same LabVIEW code via a serial-port interface. Prior to use, zero-point adjustment of the piezo servo-controller was carried out, as described in the manual and the LabVIEW-control tested against the vendor application software MikroMove (Ver. 2.4.06, Physik Instruments GmbH, Germany). A feedback algorithm is implemented in the LabVIEW code to perform controlled force or controlled strain tests (see the Appendix for details). The optical fiber and the piezo are mounted on the microscope stage using two separate sets of three-axis translation stages with micrometer precision from Thorlabs Inc. (USA) and Holmarc Opto-Mechatronics Pvt. Ltd. (India). An aluminium box is used to enclose the parts mounted on the microscope stage to minimize disturbances due to air currents.

B. Methods, calibration, and tests

1. Preparation of cantilevers

For our calibration tests, we used optical fibers with etched as well as unetched tips (see Figs. 2(a) and 2(b)). The

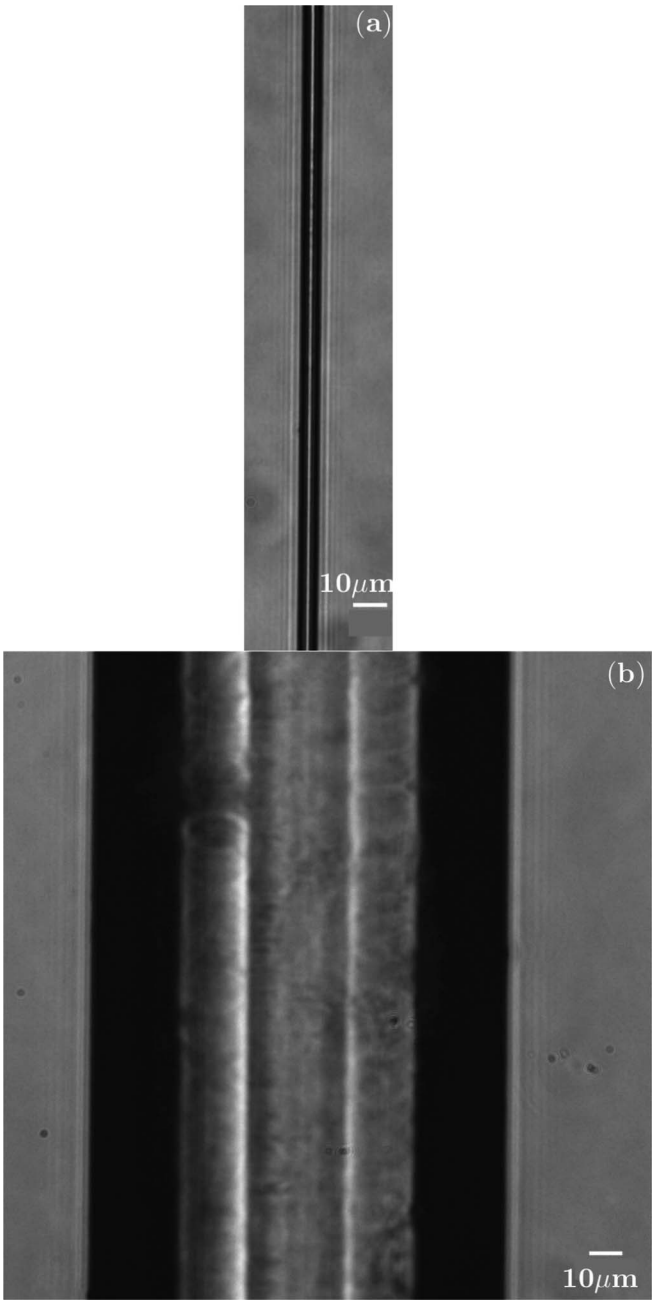

FIG. 2. (a) Etched fiber of diameter ∼8.5 μm. (b) Unetched fiber of diameter ∼124 μm.

time required for etching the fiber varied with the required diameter and the age of the hydrogen fluoride (HF, Merck, India) solution used. For etching the fiber, the required length of the fiber was dipped into freshly prepared solutions of HF. For example, to obtain an etched fiber with a diameter ∼10 μm, the following concentrations of HF were used in the sequence: 48% for 30 min, 25% for 25 min, and 15% for 15 min, followed by a rinse with de-ionised water. The acid is gently stirred using a magnetic stirrer during the etching process. This method produces nearly uniform cylindrical cantilevers with a taper which is less than 1 μm over a length of 15 mm. After etching, the tip is cut using a scalpel to obtain a nearly circular aperture (confirmed by observing the profile of the emergent light). The length of the fiber is measured under a

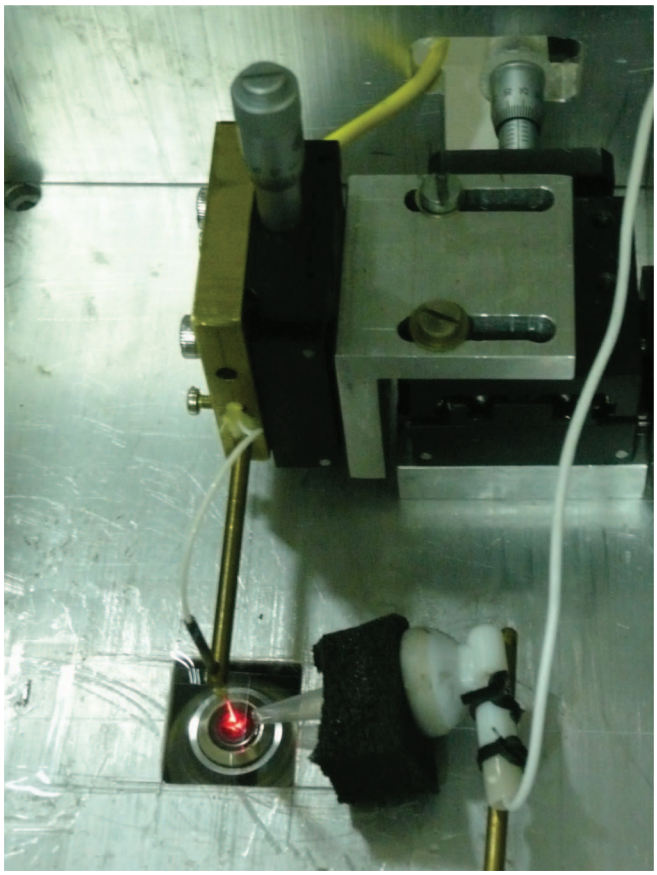

FIG. 3. The setup used for testing simple harmonic motion of the fiber tip.

stereo-microscope using a Vernier calliper with a least count of 20 μm and the diameter is measured using the microscope and the CCD camera, with an accuracy better than a micron.

2. Calibration and linearity test of the cantilever

The resonance frequency of the cantilever in air was measured by exciting it using sound waves. The waves emanating from an earphone speaker were concentrated onto the tip of the cantilever using a conical tube, as shown in Fig. 3. The speaker was excited using a sinusoidal signal from a function generator (33220A, Agilent Corp., USA). The aperture of the fiber was imaged using the CCD camera. The time-period of oscillation is much smaller than the exposure time chosen for the camera, which produces "dumbell"-shaped intensity patterns in the recorded images (see Fig. 4(a), inset). The distance $2\gamma_0$ between the intensity maxima is measured as a function of the frequency of the sinusoidal signal and the resonance frequency is determined from the amplitude-frequency curves, with an accuracy of ± 1 Hz.

In order to test for linearity, an etched fiber of length $l = 19.6$ mm and diameter $d = 14\,\mu$m was oscillated using sound waves. In Fig. 4(a), a plot of the resonance frequency ν_r as a function of the amplitude of oscillation γ_0 of the fiber tip is shown. The resonance frequency ($\nu_r = 40$ Hz) is found to be independent of the amplitude within the tested range of 25.3–69.1 μm.

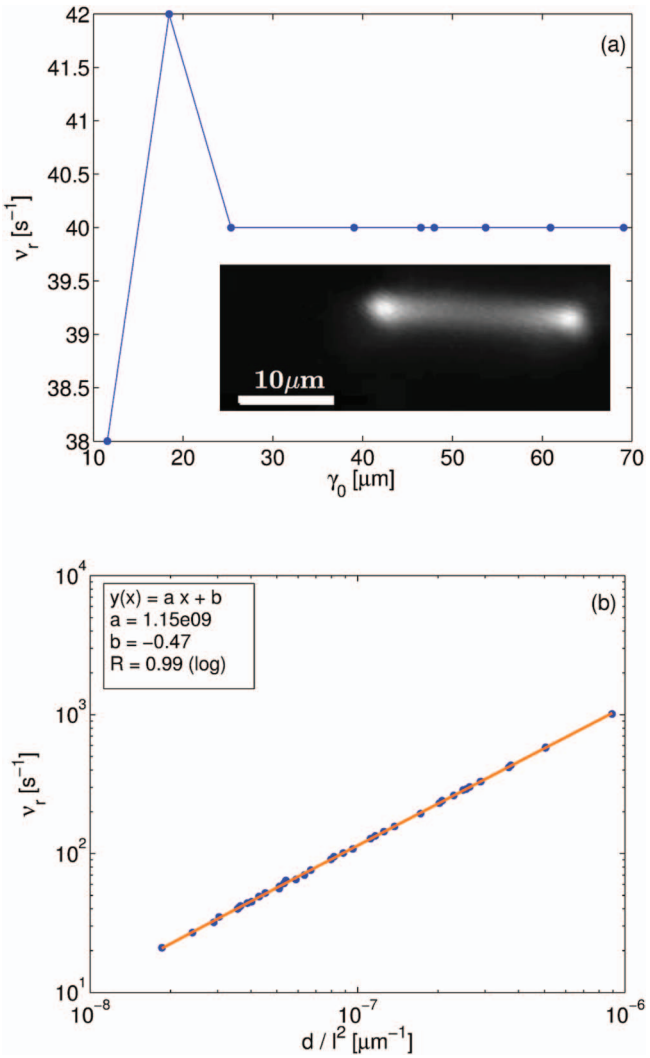

FIG. 4. (a) Plot of the resonance frequency ν_r as a function of the amplitude of oscillation γ_0 of the fiber tip. The image of the fiber tip at resonance is shown in the inset. (b) Plot of ν_r as a function of d/l^2, where d is the diameter of the fiber and l is its length.

We compared the experimentally obtained resonant frequency data with the theoretical expression for an ideal cantilever. We use the expression[28] for the smallest characteristic frequency of transverse oscillations of a rod clamped at one end with the other end free:

$$\omega_{min} = \frac{3.52}{l^2}\sqrt{\frac{EI}{\rho S}}. \quad (1)$$

Here $I = \pi d^4/64$ is the area moment of inertia of the rod, $S = \pi d^2/4$ is the cross-sectional area, $\rho = 2.297 \times 10^3$ kg/m^3 is the density of the glass fiber (measured by weighing pieces of fiber using a microbalance). The measured value $\omega_{min} = 2\pi\nu_r = 251.33$ rad/s was substituted in Eq. (1), to obtain a Young's modulus of $E = 141.91$ GPa. We note that the measured value of E is roughly double of the value ("about 73 GPa") provided by the manufacturer. The resonance frequency of oscillation depends on the length and diameter of the fiber in the form $\nu_r \propto d/l^2$. In Fig. 4(b), we show this proportionality for a set of fibers with lengths in the range of 9.7–24.3 mm and diameter in the range of 6.5–124.5 μm. This agreement between the measured and the estimated values shows that the cantilever spring constant can be accurately estimated from a measurement of its length and diameter once the material is characterized, i.e., its Young's modulus is determined.

3. Camera-based detection

The pixel resolution of the CCD camera was calibrated using a microscope calibration scale with a least count of 10 μm (AX0001, OB-M, Olympus Corp., Japan). Here on, unless otherwise specified, we have used the 40 × /0.5 objective. At this magnification, the calibration factor was found to equal 0.194 μm per pixel. The image of a well-cut static fiber produces a nearly-Gaussian intensity profile on the camera. A Region of Interest (ROI) larger than the beam profile is chosen when recording the data. The intensity-weighted centroid of the fiber in the image plane is then calculated as $(x_{cm}, y_{cm}) \equiv (\sum_i I_i x_i/I, \sum_i I_i y_i/I)$, where $I = \sum_i I_i$, and x_i and y_i are the x and y positions of the ith pixel. The background intensity can affect the calculated position. To avoid this, the background intensity value I_b (the average value along the edge of the ROI) was used as a cutoff by setting $I_i = 0$ for $I_i < I_b$.

In order to estimate the noise in this detection method we imaged a "rigid" cantilever, i.e., a short segment of an unetched optical fiber with the tip stuck to an aluminum block. A drop of immersion oil (Immersol 518F, Carl Zeiss AG, Germany) was placed on a coverslip above the objective with the tip of the fiber dipping into it, to reduce scattering due to any imperfections in the cut. The position of the cantilever was recorded as a time series at 10 Hz for 300 s. The standard deviation for measured displacements of the x or y coordinate gives an estimate of the error in the detection method. A plot of $(\Delta x_{cm})_{RMS}$ as a function of the total magnification M_o is shown in Fig. 5. As can be seen from the plot, the best spatial resolution was obtained at $M_o = 250$, with an error ~1 nm.

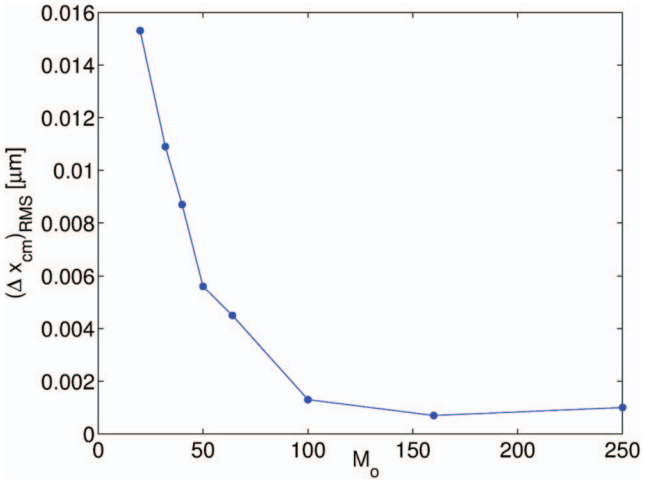

FIG. 5. Plot of the root-mean-square centroid displacement $(\Delta x_{cm})_{RMS}$ of a rigidly mounted unetched fiber, recorded using a camera as a function of the total magnification M_o.

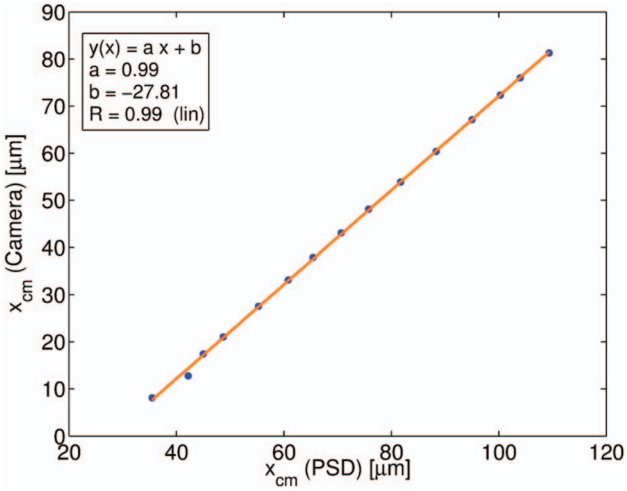

FIG. 6. Plot of the centroid x_{cm} coordinate of the fiber tip recorded by the PSD as a function of the x_{cm} coordinate calculated from the camera images.

4. Position-Sensitive Detector (PSD)

The resolution of the PSD, with a resistance length (inter-electrode distance) of 5700 μm and 12-bit resolution for the A/D conversion is 5700 μm/2^{12} = 1.39 μm. When the light spot is imaged through a microscope, the resolution equals 1.39 μm/M_o (we use $M_o = 40$). For checking the linear range of the PSD, an unetched fiber was mounted on the microscope using the translation stage. Position information was recorded using both the PSD software and the camera simultaneously for each displacement step made using the translation stage. In Fig. 6, the position of the centroid x_{cm} coordinate tracked using the camera is plotted as a function of the PSD x_{cm} coordinate and is found to be proportional. The position resolution was found to be independent of location within the active area of the PSD and the incident light level within the operating range.

5. Piezoelectric transducer

A carboxylate-modified fluorescent microsphere (FluoSpheres, Invitrogen Corp., USA) of 2 μm diameter was stuck to the tip of a 24 gauge injection needle which was magnetically attached to the piezo actuator and imaged using the camera. Images of the bead were recorded for step displacements of the piezo actuator. In Fig. 7(a), the centroid coordinate y_{cm} of the spot as calculated from the camera images is plotted vis-a-vis the commanded piezo displacement in steps of 0.1 μm. In Fig. 7(b), y_{cm} is plotted for piezo displacements with a step size 0.01 μm. The fit is found to be linear and the piezo actuator motion agrees with spot-tracking using the camera for displacements $\gtrsim$ 0.01 μm.

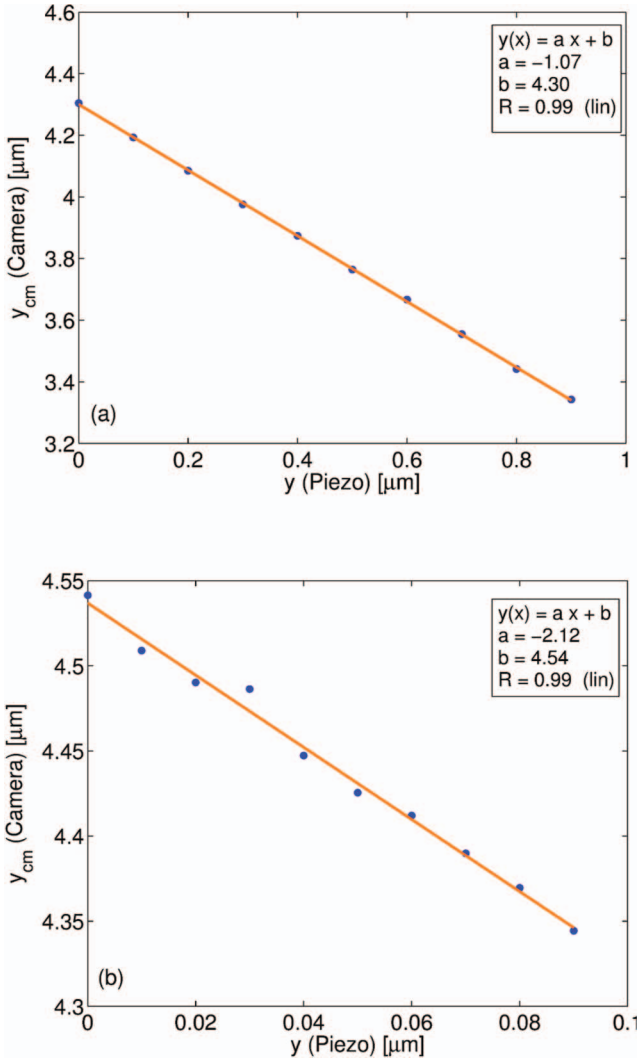

FIG. 7. Plot of the centroid y_{cm} coordinate of the bead attached to the piezo, calculated from camera images as a function of the commanded piezo displacement, in steps of (a) 0.1 μm and (b) 0.01 μm.

III. APPLICATIONS

A. Experiments with a bacterial suspension

The dynamics of active matter is an important area of non-equilibrium statistical physics and bacterial suspensions have often been used as model systems.[29] Typical experiments are performed by analyzing the response of latex beads trapped using an optical tweezer.[30] We demonstrate below that a simpler system with only an etched optical fiber mounted on a translation stage above the microscope objective, with a camera (or QPD) for imaging, can be used for such studies.

For these experiments we used an etched fiber with a length l = 19.6 mm and a diameter d = 11.2 μm, which has a spring constant $k = 1.78 \times 10^{-4}$ N/m. The bacterial strain (RP5232) of *Escherichia coli* bacteria which are predominantly "swimmers," was cultured in tryptone medium (Bacto Tryptone, BD Biosciences, USA) for about 6 h at 30 °C with shaking. Further details concerning the protocol for culturing the bacteria and preparation of the relevant medium are discussed in a laboratory manual.[31] In Figs. 8(a) and 8(b), we show plots of the centroid displacement components of the tip of the fiber normalized by their root-mean-square values $[\Delta x_{cm}/(\Delta x_{cm})_{RMS}, \Delta y_{cm}/(\Delta y_{cm})_{RMS}]$, for the medium alone and for the bacteria in the medium, recorded at 10 Hz for 300 s. We note the relatively larger forces exerted by the bacteria during random collisions with

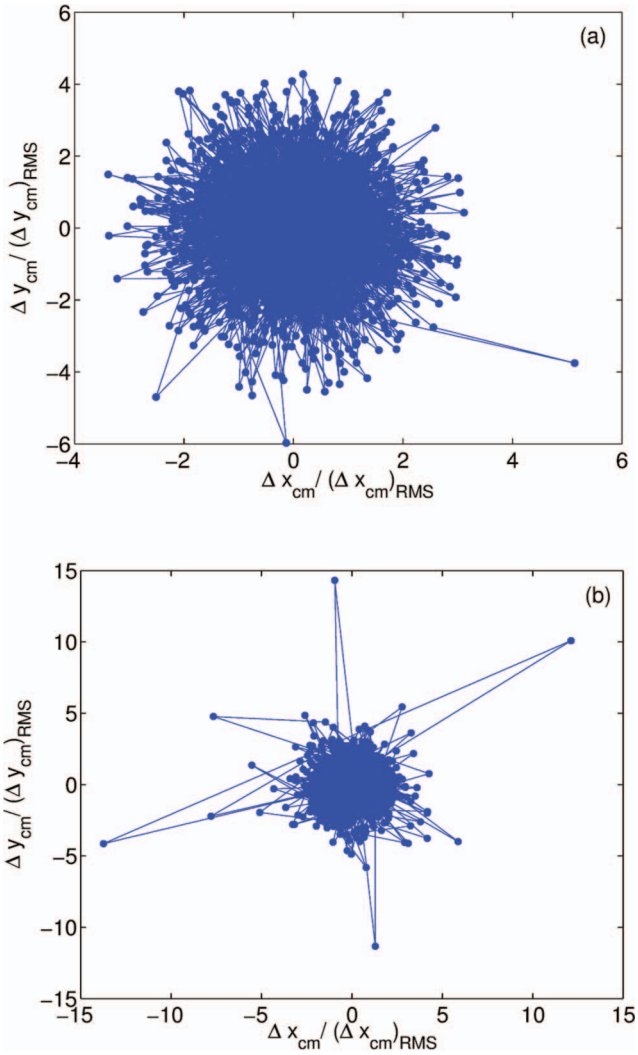

FIG. 8. (a) Plot of the normalized centroid displacements Δx_{cm} and Δy_{cm} of the etched fiber recorded using the camera, with the tip immersed in (a) tryptone medium (b) tryptone medium containing *E. coli* bacteria.

the fiber tip in Fig. 8(b). The kurtosis for x-displacements, $K_{\Delta x_{cm}} \equiv \langle(\Delta x_{cm})^4\rangle / \langle(\Delta x_{cm})^2\rangle^2$ showed stark differences in magnitude, with $K_{\Delta x_{cm}} = 3.24$ for the medium (for a stochastic variable x having a Gaussian distribution,[32] $K_x = 3$) and $K_{\Delta x_{cm}} = 25.47$ for the bacteria in the medium. An estimate of the average magnitude of the force exerted on the cantilever was obtained by calculating the average magnitude of the displacement $\langle|\Delta x_{cm}|\rangle$ for the two cases and multiplying with the spring constant, to get $\langle|F_x|\rangle = 4.7 \times 10^{-12}$ N for the bacteria in the medium and $\langle|F_x|\rangle = 2.23 \times 10^{-12}$ N for the medium alone.

B. Extensional rheology of polymer melts

In the field of extensional rheology,[18,19,33] several devices such as the FiSER,[21,22] the CaBER,[23,24] microplate-based rheometer,[10–12] etc., have been used to measure rheological properties of materials under extension. The working principle of these devices is as follows: The material under study is sandwiched between two plates, one of which moves with a specified strain (or strain-rate), and a force sensor on the other (stationary) plate is used to measure the axial force exerted by the material. In the FiSER, a laser micrometer attached to the moving plate is used to measure the mid-plane diameter of the filament. An exponential strain with a constant extensional strain-rate is commanded to the moving plate. The axial force, the mid-plane diameter of the filament, and the extensional strain-rate are then used to calculate the uniaxial extensional viscosity of the material. In a recent version[34] of the FiSER, a feedback-loop algorithm has been incorporated. In the CaBER, a step-strain (or exponential strain) profile is commanded to the moving plate and constitutive modeling is used to infer the axial force on the stationary plate. A recent version[35] of the CaBER incorporates a force-sensor, permitting real-time measurements of the force. Both the FiSER and the CaBER are relatively large-scale devices which require tens of microliters of the sample for tests. By contrast, the MER requires only a few picoliters of the sample; an attribute which can be very useful for characterizing scarce or expensive liquids, especially biological fluids.

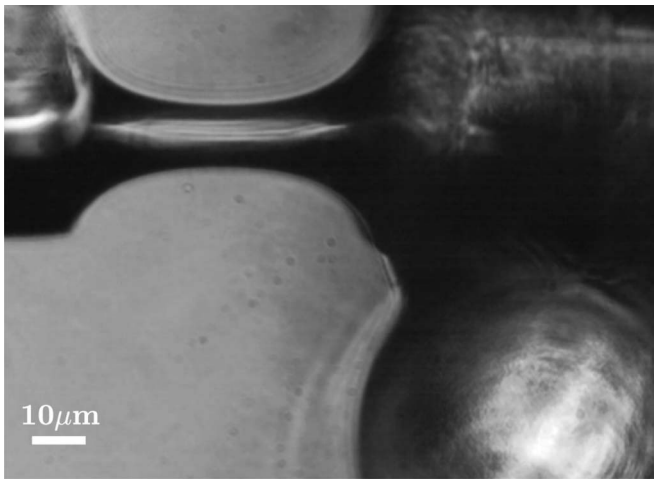

FIG. 9. A filament of polydimethylsiloxane (PDMS) between two flat surfaces. The (defocused) laser spot exiting the fiber tip can be seen at the bottom of the image.

Extensional rheometry at microscopic scales is an important application of the MER. The aim of these experiments is to measure rheological properties of materials such as polymer melts, biopolymer gels, pastes, etc., subject to an uniaxial extensional flow. In order to perform experiments in constant strain or constant force mode, a feedback-loop algorithm is utilized (see the Appendix). The material is formed into a filament between a syringe needle attached to the piezo and the tip of the cantilever. In most of our experiments, we used curved surfaces at the ends of the filament, however, for a few experiments (not reported in this paper) of flat end-surfaces were constructed by gluing a short segment of the same optical fiber used for the cantilever to the syringe needle and to the tip of the cantilever, with about 1 mm projecting out of the needle. In Fig. 9, we show a photograph of this arrangement.

In the constant force mode, the deflection of the cantilever is kept constant and the response strain and time-varying cross-sectional area of the filament are monitored, while in the constant strain mode, the deflection of the cantilever and the cross-sectional area are monitored. Details

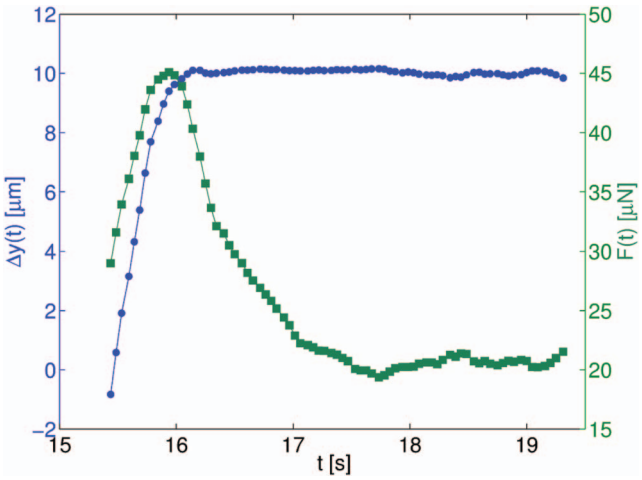

FIG. 10. A plot of the extension $\Delta y(t)$ (solid blue circles) and the force $F(t)$ (solid green squares) as a function of the elapsed time t, from a test with a commanded step of 10 μm imposed on a polydimethylsiloxane (PDMS) filament with initial length $L_0 = 35.7\ \mu$m.

concerning the formulae used to calculate the force and the strain may be found in the Appendix. The (transient) uniaxial extensional modulus of the material is defined as the ratio of the extensional stress (the time-varying force divided by the time-varying cross-sectional area of the mid-portion of the filament) and the extensional strain. We may also command an exponential strain to the piezo and use a high-speed camera to record the mid-plane diameter of the thinning filament, which may be used to infer the extensional viscosity of the material.

To validate our feedback-loop algorithm, we show results from constant extension (or constant strain) experiments using polydimethylsiloxane (PDMS, Anton Paar GmbH, Austria), with a commanded extension of 10 μm. The cantilever had a length $\ell = 15.1$ mm and a diameter $d = 125\ \mu$m. In Fig. 10, a plot of the extension $\Delta y(t)$ and the response force $F(t)$ as a function of the elapsed time t is shown. The plot shows that the extension (or strain) equilibrates to the commanded value within 1 s, and the force exerted by the filament decays over a longer period of time. For incompressible materials subject to uniaxial extension in the linear viscoelastic regime, it can be shown[36] that $\lim_{\epsilon\to 0} G_u(\epsilon) = 3 \lim_{\gamma\to 0} G(\gamma)$, where G_u is the uniaxial extensional modulus, $|G| \equiv \sqrt{G'^2 + G''^2}$ is the shear modulus (G' and G'' are the in-phase and out-of-phase components of the modulus from an oscillatory shear test), ϵ is the uniaxial extensional strain and γ is the shear strain. A stress-controlled rheometer (MCR-301, Anton Paar GmbH, Austria) with 50 mm diameter cone-plate geometry was used to estimate the value of the shear modulus ($G \approx 7800$ Pa) at shear strains $\gamma \lesssim 0.01$. For values of the extension $\Delta y(t) \lesssim 10\ \mu$m (or $\epsilon \lesssim 0.28$), we find a negligible change in the mid-plane diameter of the filament and assume that its cross-sectional area is a constant. The calculated extensional modulus (using the equilibrated value of the force $F \approx 22.7\ \mu$N) is found to equal $G_u \approx 61\,000$ Pa, i.e., $G_u/G = 7.82$. For viscoelastic materials such as PDMS, the filament is subject to surface tension forces, elastic stresses, gravity (which is usually negligible), viscous forces, and inertia. The complete force-balance equation for the filament may be found in some earlier Refs. 22 and 37. In our proof-of-principle test, we do not take into account effects due to curvature of the filament or the inertia, and thereby ignore contributions to G_u from such terms. We have also assumed that our deformation is purely uniaxial, which may not be true near the ends of the filament. In a future study, we aim to reduce this discrepancy in our measurements, by explicitly taking into account effects due to surface tension and inertia and with the inclusion of results for a Newtonian fluid.

IV. DISCUSSION

The MER has several features in common with single-molecule force spectroscopy devices such as AFM, optical tweezers, and magnetic tweezers. AFM cantilevers work in the direction perpendicular to the specimen plane, while the MER cantilever moves in the plane of the specimen, which is also the focal plane of the optical microscope. This facilitates imaging of the sample along with simultaneous force-measurement. In many AFMs, the light of a laser diode is focused onto the back of the cantilever and the reflection angle is measured, which decreases the accuracy of the position measurement[38] whereas in the MER, the tip of the cantilever is imaged directly. While the AFM is suitable for surface-scanning, high-force pulling, etc., the MER is well-suited for pulling cells such as neurons or muscle cells with simultaneous imaging, measuring forces exerted by active suspensions, and extensional rheology of viscoelastic materials. The working principles of optical tweezers and the MER are quite different: Optical tweezers[4,5] use focused laser beams to hold and manipulate sub-micron sized particles, while the MER utilizes a piezo to push or pull microscale samples. Magnetic tweezers[6,7] utilize the force due to an external magnetic field to manipulate molecules stuck onto magnetic particles which may be displaced. In an earlier work, Cluzel *et al.*[13] used an etched optical fiber-based force transducer setup which is similar to the MER. The advantages of the MER in comparison with the Cluzel *et al.*[13] apparatus are that simultaneous imaging and force measurements are possible using a feedback mechanism which permits different modes of operation at a higher temporal resolution. Glass micro-needles/microplates[8,10,11] have also been used to apply forces on cells and the technique is essentially similar to that used for the MER. Microplates are difficult to calibrate and their fabrication requires special machinery. Also, the shape of the cantilever is complicated, vis-a-vis the MER. For the case of micro-needles, no laser is used and the deflection of the needle as well as the extension produced in the sample are measured by optical microscopy. Due to this limitation, spatial accuracy is restricted.

A comparison of the spatiotemporal resolution, and the force and displacement ranges of these devices may be found in Table I. The MER may be used for a wide range of applications including the measurement of the extensional viscosity and extensional moduli of biofluids, "tailor-made" model liquids, yield-stress materials and other complex fluids, measure the surface tension of materials, measure the forces exerted by active suspensions, map extensional stresses in the deforming

TABLE I. A comparison of some common force-spectroscopy techniques with the MER. The data for Atomic Force Microscopes (AFM), Optical Tweezers (OT), and Magnetic Tweezers (MT) are taken from Ref. 1.

	AFM	OT	MT	MER
Spatial resolution (nm)	0.5–1	0.1–2	5–10	∼1
Temporal resolution (s)	10^{-3}	10^{-4}	10^{-2}–10^{-1}	10^{-6}
Force range (pN)	10–10^4	0.1–10^2	10^{-3}–10^2	1–10^8
Displacement range (nm)	0.5–10^4	0.1–10^5	5–10^4	10–10^5

material via birefringence or by seeding the material with tracer particles and imaging the flow-field, oscillatory extensional rheometry, among other potential applications.

ACKNOWLEDGMENTS

We thank A. Lele, S. Pinge, A. Nisal, and V. Singh for discussions, J. Armitage for supplying the bacterial strain and protocol for usage. P.A.P. thanks the Department of Biotechnology, India for financial support.

APPENDIX: FEEDBACK LOOP AND DEFINITIONS USED

1. Feedback loop

A user-friendly software for the MER has been written using LabVIEW. The software allows the user to select from the following modes of operation: constant strain mode and constant force mode. The user-selected mode is implemented via a feedback-loop algorithm. A screen-shot of the Front Panel of the code is shown in Fig. 11. The user selects the mode of operation and supplies as input, the desired value of the extension (or force), the diameter and length of the cantilever, and the initial filament length after loading the sample and allowing the filament to stabilize. The code implements the desired mode of operation and outputs the calculated spring constant, and the current values of the PSD and piezo positions. A graphical display shows the current values of the force and the strain as a function of the elapsed time.

FIG. 11. A screenshot of the MER Controller software, which permits operation of the device in constant force or constant strain modes via a feedback-loop algorithm.

2. Definition of force and strain

We now discuss our definition of the force and the strain which has been implemented within the feedback-loop code. It is important to note that for extensional rheology experiments, the act of loading a picoliter volume of sample onto the cantilever and forming the filament, deflects the cantilever by a certain amount, i.e., a pre-loaded force F_0 is imposed on the cantilever due to surface forces and/or residual elastic stresses in the filament, prior to start of the experiment. The value of F_0 must be estimated by the user as a function of the initial filament length L_0, for each material under study. For the constant force mode, we assume that such a procedure has been carried out prior to use. Assuming that the single-axis piezo traverses the y-axis, the time-dependent force is then defined as $F(t) \equiv -k(y_{PSD}(t) - y_{PSD,\,BL})$ where k is the calculated spring constant, $y_{PSD}(t)$ is the current position of the PSD, and $y_{PSD,\,BL}$ refers to the PSD position Before Loading (subscript BL) the sample. The "true" force on the sample may be calculated as $F(t) - F_0$. However, for the constant strain mode, the force being a measured quantity, requires no such initial procedure. Unlike the force, the strain imposed on the sample must be calculated after the filament has stabilized, i.e., after loading the sample. Therefore, the appropriate tensile strain is defined as $\epsilon(t) \equiv \Delta y(t)/L_0 = [(y_{PZ}(t) - y_{PZ,\,AL}) - (y_{PSD}(t) - y_{PSD,\,AL})]/L_0$, where $y_{PZ}(t)$ is the current position of the piezo (subscript PZ) and $y_{PSD,\,AL}$ refers to the PSD position After Loading (subscript AL) the sample.

[1] K. Neuman and A. Nagy, Nature Methods **5**, 491 (2008).
[2] G. Binnig, C. Quate, and C. Gerber, Phys. Rev. Lett. **56**, 930 (1986).
[3] O. Sahin, S. Magonov, C. Su, C. Quate, and O. Solgaard, Nature Nanotechnol. **2**, 507 (2007).
[4] A. Ashkin, Phys. Rev. Lett. **24**, 156 (1970).
[5] A. Ashkin, Proc. Natl. Acad. Sci. U.S.A. **94**, 4853 (1997).
[6] T. Strick, J. Allemand, D. Bensimon, A. Bensimon, and V. Croquette, Science **271**, 1835 (1996).
[7] C. Haber and D. Wirtz, Rev. Sci. Instrum. **71**, 4561 (2000).
[8] R. Bernal, P. Pullarkat, and F. Melo, Phys. Rev. Lett. **99**, 018301 (2007).
[9] T. Dennerll, P. Lamoureux, R. Buxbaum, and S. Heidemann, J. Cell Biol. **109**, 3073 (1989).
[10] N. Desprat, A. Guiroy, and A. Asnacios, Rev. Sci. Instrum. **77**, 055111 (2006).
[11] P. Fernández, P. Pullarkat, and A. Ott, Biophys. J. **90**, 3796 (2006).
[12] O. Thoumine and A. Ott, J. Cell Sci. **110**, 2109 (1997).
[13] P. Cluzel, A. Lebrun, C. Heller, R. Lavery, J. Viovy, D. Chatenay, and F. Caron, Science **271**, 792 (1996).
[14] S. Smith, L. Finzi, and C. Bustamante, Science **258**, 1122 (1992).
[15] D. Simson, F. Ziemann, M. Strigl, and R. Merkel, Biophys. J. **74**, 2080 (1998).
[16] D. Cheneler, M. Ward, M. Adams, and Z. Zhang, Sens. Actuators B **130**, 701 (2008).
[17] S. Jericho, M. Jericho, T. Hubbard, and M. Kujath, Rev. Sci. Instrum. **75**, 1280 (2004).
[18] H. Barnes, J. Hutton, and K. Walters, *Introduction to Rheology* (Elsevier, 1989).
[19] G. McKinley and T. Sridhar, Annu. Rev. Fluid Mech. **34**, 375 (2002).
[20] C. Petrie, J. Non-Newtonian Fluid Mech. **137**, 15 (2006).
[21] T. Sridhar, V. Tirtaatmadja, D. Nguyen, and R. Gupta, J. Non-Newtonian Fluid Mech. **40**, 271 (1991).
[22] P. Szabo, Rheol. Acta **36**, 277 (1997).
[23] A. Bazilevsky, V. Entov, and A. Rozhkov, in *Third European Rheology Conference*, edited by D. Oliver (Elsevier, New York, 1990), pp. 41–43.
[24] G. McKinley and A. Tripathi, J. Rheol. **44**, 653 (2000).
[25] J. Meissner, Annu. Rev. Fluid Mech. **17**, 45 (1985).
[26] M. Sentmanat, B. Wang, and G. McKinley, J. Rheol. **49**, 585 (2005).

[27]A. Bausch, F. Ziemann, A. Boulbitch, K. Jacobson, and E. Sackmann, Biophys. J. **75**, 2038 (1998).
[28]L. Landau and L. Lifshitz, *Theory of Elasticity* (Pergamon Press, Oxford, 1986).
[29]S. Ramaswamy, Annu. Rev. Condens. Matter Phys. **1**, 323 (2010).
[30]J. Jass, S. Schedin, E. Fallman, J. Ohlsson, U. Nilsson, B. Uhlin, and O. Axner, Biophys. J. **87**, 4271 (2004).
[31]J. Sambrook and D. Russell, *Molecular Cloning: A Laboratory Manual* (Cold Spring Harbor Laboratory Press, Cold Spring Harbor, NY, 2001).
[32]J. Kenney and E. Keeping, *Mathematics of Statistics* (D. Van Nostrand Company, New York, 1954).
[33]C. Petrie, J. Non-Newtonian Fluid Mech. **137**, 1 (2006).
[34]J. Marín, J. Huusom, N. Alvarez, Q. Huang, H. Rasmussen, A. Bach, A. Skov, and O. Hassager, J. Non-Newtonian Fluid Mech. **194**, 14 (2013).
[35]C. Klein, I. Naue, J. Nijman, and M. Wilhelm, Soft Mater. **7**, 242 (2009).
[36]J. Dealy and K. Wissbrun, *Melt Rheology and Its Role in Plastics Processing - Theory and Applications* (Springer, 1999).
[37]P. Szabo and G. Mckinley, Rheol. Acta **42**, 269 (2003).
[38]H. Butt and M. Jaschke, Nanotechnology **6**, 1 (1995).